Blind Calibration of Timing Skew in Time-Interleaved Analog-to-Digital Converters

Vijay Divi, *Member, IEEE*, and Gregory W. Wornell, *Fellow, IEEE*

***Abstract*—The performance of time-interleaved analog-to-digital converters is often significantly degraded by timing mismatch errors. We develop methods for performing blind calibration of such converters, i.e., for estimating the unknown time-skew parameters and for performing signal reconstruction from these estimates. The methods are low in complexity and allow for accurate calibration in systems with large numbers of converters, provided that the skews are sufficiently small in magnitude. We also present modifications to calibrate gain mismatch as well as adaptive sequential methods of implementation. Performance and complexity analysis is provided to support the viability of the methods.**

***Index Terms*—Adaptive systems, analog-digital conversion (ADC), calibration, parameter estimation, signal reconstruction, signal sampling.**

I. Introduction

As new applications require the use of higher performance analog circuitry, two major problems arise. Often, the analog components cannot realize the necessary system specifications in a power and cost-efficient manner. Also, process variations in chip production can require larger design margins to keep chip yields high.

With digital component performance scaling aggressively, large benefits can be achieved by finding digital methods to compensate for inadequate analog circuit performance and by allowing the system designer to relax analog circuit constraints. Advantages can include a reduction in cost, power consumption, and size, along with providing an increase in speed, accuracy, testability, and system robustness. In this paper, we focus on high-speed sampling circuits and develop calibration methods that mitigate the effects of the problems that arise.

As applications become more advanced, a single state-of-the-art analog-to-digital converter (ADC) may be insufficient to handle the system sampling requirements. The single converter may not be able to sample fast enough or may consume a large amount of power in order to do so. At high sampling rates, time-interleaved analog-to-digital converters (TIADCs) offer, in principle, an attractive method of sampling by distributing the load across many converters [1].

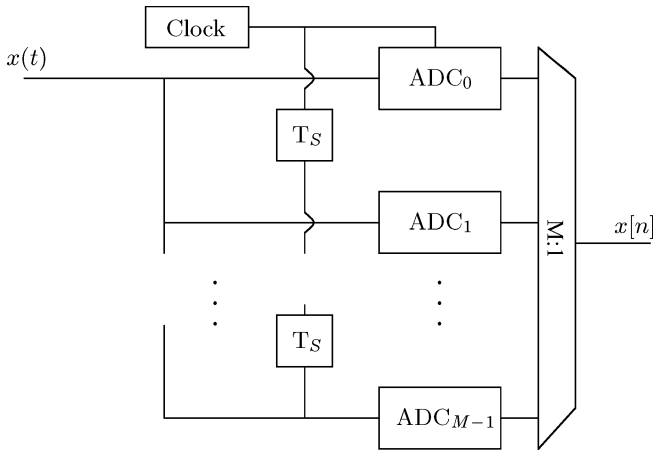

Fig. 1. Ideal time-interleaved ADC system with M converters.

TIADCs operate in a round-robin manner. In a system of M converters, to realize a system sampling period of T_s, each converter operates with sampling period MT_s and a spacing of T_s between consecutive converters, as seen in Fig. 1. Thus, the sampling rate required by the ADCs in the system is reduced by a factor of M, allowing for a lower amount of overall power consumption and a greater control over sampling accuracy.

Although TIADCs may avoid some of the problems presented by using a single high-speed ADC, they also introduce a new set of problems. In particular, mismatches among the ADCs in a time-interleaved system lead to inaccurate sampling [2], [3]. One significant source of error in TIADCs is timing skew, which can be caused by signal path length differences. Although system designers try to ensure that the clock signal and input signal travel uniform distances to each converter, restrictions in the physical layout introduce unavoidable errors. Even when clock and signal paths are precisely matched, variations in gate delays also result in timing skew. Other nonlinear mismatches can be modeled as gain and amplitude offset variations among the converters [4]; however, a variety of circuit-based matching techniques exist for the minimization of such errors [5]. For this reason, we focus on signal recovery when only timing skews are unknown in the system and assume that the gains and amplitudes are calibrated. The general case is examined briefly in this paper and studied in more detail in, e.g., [6].

There are two general approaches to system calibration. The first approach is to incorporate a known signal in the input in order to facilitate direct estimation of the unknown

Manuscript received June 04, 2008; revised February 23, 2009. Current version published May 15, 2009. This work was supported in part by the SRC Focus Center for Circuit and System Solutions (C2S2) under Contract 2003-CT-888, in part by MIT Lincoln Laboratory, and in part by NEC Corporation. This work was presented in part at the International Conference on Acoustics, Speech, and Signal Processing (ICASSP) Las Vegas, NV, April 2008. The associate editor coordinating the review of this manuscript and approving it for publication was Dr. Anand Babak.

The authors are with the Department of Electrical Engineering and Computer Science, Massachusetts Institute of Technology, Cambridge, MA 02139 USA (e-mail: vdivi@mit.edu; gww@mit.edu).

Color versions of one or more of the figures in this paper are available online at http://ieeexplore.ieee.org.

Digital Object Identifier 10.1109/JSTSP.2009.2020269

timing-skews and other parameters [7], [8]. The various implementations of such a method may require extra hardware, decrease the sampling resolution, or cause system delays by requiring operation of the converter to be interrupted.

The second approach is to perform blind recovery using only the ADC outputs. Such methods may use oversampling and take advantage of the excess bandwidth in the system to enable calibration. The primary focus is to perform calibration without placing significant restrictions on the input class and while keeping computation complexity low; however, it is often the case that one of these goals is not achieved.

There has been growing interest in such blind methods for time-interleaved ADCs. In addition to our own work [6], [9], [10], upon which the present development is based, some of the recent papers from parallel efforts include [5], [11]–[17]. In [11], the timing-skew estimation involves a exhausted search through the parameter space, requiring a large amount of complexity. Other approaches impose a stationarity property on the input to reduce complexity. The computation required in [12] is still high; while the calibration method in [13] for $M = 2$ converters has low complexity and can be efficiently implemented in hardware. An alternate 2-ADC blind calibration method that does not require input stationarity is proposed in [5]. Although the calibration algorithm has low complexity, it requires large amounts of oversampling and does not generalize to $M > 2$ converters. The frequency domain approaches presented in [14], [15] perform well with little oversampling; however, low-complexity implementations are restricted to systems with few converters ($M = 2$ in [14], $M = 4$ in [15]).

Calibration for systems with larger numbers of converters has been developed by the authors in [9]. By using Taylor series approximations to linearize the problem, vast advances have been made that reduce the complexity while providing accurate parameter estimates. This approach has also been explored in other parallel works [16], [17]. In general, these calibration schemes provide methods for estimating the time-skew parameters; from these estimates, multiple methods have been developed for efficient input signal reconstruction [18]–[22].

In this paper, we develop and analyze methods for blind calibration and signal reconstruction in TIADCs with many converters, extending the results of [9] and [22]. We examine the small timing mismatch case, which is typical of high-resolution architectures where time-skews are generally small relative to the system sampling period, and develop a method for blind calibration in this setting. We first derive a linear approximation to the input reconstruction formula. This approximation leads to a new method for mismatch estimation by imposing a bandlimited restriction on the input reconstruction. By performing all operations in the time-domain, the method maintains low complexity even for systems with many converters. The calibration method both estimates the converter skews and creates a reconstruction of the input sampled on a uniform grid, provided that the overall system sampling rate is above the input Nyquist rate. Additional techniques are also presented for reconstruction in the high noise setting.

The paper is organized as follows. In Section II, we present the timing mismatch setup and develop a least-squares based calibration algorithm for estimating the time-skew parameters. Using these time-skew estimates, we present multiple methods of input signal recovery in Section III. The simulation results from each of the estimation methods is then presented in Section IV. We conclude with remarks about future work.

II. Timing Mismatch Calibration

In this section, we first describe the time-interleaved framework. We then present a reconstruction method for recovering uniform samples of the input when the time-skews are known. Using this reconstruction, we develop a least-squares method for estimating the unknown time-skews. We finish by generalizing to systems where nonuniform gains also exist.

The TIADC input $x(t)$ is modeled as a deterministic bandlimited signal with cutoff frequency Ω_c, i.e., the continuous time Fourier transform $X(j\Omega) = 0$ for $\Omega_c < |\Omega| \leq \pi$. The overall sampling period T_s of the system is chosen to ensure that the sampling rate strictly exceeds the Nyquist frequency, i.e., $T_s < \pi/\Omega_c$, thus creating some amount of excess bandwidth.

We model the output of the ith constituent ADC as

$$y_i[n] = x(nMT_s + iT_s + \tau_i) + w_i[n] \tag{1}$$

where the τ_i model the unknown skews. We also make the assumption that the timing skews are relatively small, e.g., not more than 20% of the overall sampling period. The $w_i[n]$ represents the aggregate noise, modeled as white Gaussian whose variance primarily depends on the number of bits to which the input is quantized. For ease of analysis, we assume the input is quantized with high-resolution, $w_i[n] \approx 0$; however the effects of quantization noise are considered within the subsequent simulations. Without loss of generality, we can choose an arbitrary time reference, thus we let $\tau_0 = 0$.

We use the following notation to represent the signal obtained by multiplexing the ADC outputs:

$$y[n] = y_i\left[\frac{n-i}{M}\right] n(\mathrm{mod}\ M) = i. \tag{2}$$

This received signal is also referred to as the uncalibrated signal. We can rewrite $y[n]$ in terms of the uniform samples $x[n]$ as follows. First we note that since $x(t)$ is bandlimited to Ω_c and the sampling frequency is higher than the Nyquist frequency, it can be written as

$$x(t) = \sum_m x[m]\mathrm{sinc}(t - mT_s). \tag{3}$$

Second, for $n(\mathrm{mod}\ M) = i$,

$$y[n] = x(T_s + \tau_i) + w[n] \tag{4}$$

$$= \sum_m x[m]\mathrm{sinc}\left((n-m)T_s + \tau_i\right) + w[n]. \tag{5}$$

where the sinc terms are defined with period T_s. The goal of the signal recovery problem is to estimate $x[n] = x(nT_s)$, which is bandlimited to $\omega_c = \Omega_c T_s < \pi$, as accurately as possible from the ADC outputs $y[n]$. To do this, we develop an algorithm for estimating the unknown timing skews τ_i.

A. Input Class Restrictions

Although we specify that $x[n]$ must be bandlimited, it is necessary to add additional requirements on the input class in order to ensure that accurate reconstruction can be obtained in a time-interleaved system. In particular, we restrict ourselves to the class of nontrivial input signals for which nonuniform periodic sampling (with nonzero skew) yields aliased content in the frequency band $\omega_c < \omega < \pi$, i.e.,

$$Y(e^{j\omega}) \neq 0 \quad \text{for some } \omega_c < \omega < \pi. \tag{6}$$

Without this requirement, the problem becomes ill-posed as the input signal $x(t)$ that generates output $y[n]$ may not be unique.

The calibration methods presented can also be extended to work for a larger class of signals where the aliased content due to nonuniform sampling appears in other bands of the spectrum; in this case, the algorithms can be redefined with small modifications made to the filters.

Some example subclasses of bandlimited input signals that can be accommodated include the following.

- Inputs $x(t)$ that are spectrally "full"

$$X(e^{j\omega}) \begin{cases} \neq 0 & |\omega| \leq \omega_c \\ = 0 & \omega_c < |\omega| \leq \pi. \end{cases} \tag{7}$$

  Aliasing occurs in the band $\omega_c < |\omega| \leq \pi$ and the subsequent algorithm can be used to accurately estimate the unknown timing skews.
- Passband signals with aliasing in other bands, e.g.,

$$X(e^{j\omega}) \begin{cases} \neq 0, & \frac{\pi}{2} \leq |\omega| \leq \frac{2\pi}{3} \\ = 0, & \text{otherwise.} \end{cases} \tag{8}$$

  For $M = 2$ converters, the aliasing in $y[n]$ appears in the band $\pi/3 \leq |\omega| \leq \pi/2$. The calibration algorithms we describe can be modified to handle such signals as long as the input signal band $\pi/2 \leq |\omega| \leq 2\pi/3$ is known to the system.

An example subclass of bandlimited signals that cannot be calibrated is as follows.

- Passband signals whose aliasing occurs in the passband, e.g.,

$$X(e^{j\omega}) \begin{cases} \neq 0, & \frac{\pi}{3} \leq |\omega| \leq \frac{2\pi}{3} \\ = 0, & \text{otherwise.} \end{cases} \tag{9}$$

  For $M = 2$ converters, the aliasing also appears in the band $\pi/3 \leq |\omega| \leq 2\pi/3$. Any estimate of the timing skews will yield an input reconstruction $\hat{x}[n]$ that lies in this passband; thus, the signal cannot be accurately reconstructed.

In the case of $M > 2$ ADCs, spectral content is aliased to $M-1$ locations, thus yielding a larger amount of spectrum from which the aliasing in $y[n]$ can be detectable.

B. Small Error Resampling

To motivate our estimation algorithm, we first present methods for recovering the input signal from the converter outputs when the timing skews are known. The equation for signal reconstruction from periodic nonuniform samples in the absence of noise is derived in [23]. The reconstruction for the M-ADC system is given by

$$x(t) = \gamma(t) \sum_{\alpha=-\infty}^{\infty} \sum_{i=0}^{M-1} y[M\alpha + i] \frac{a_i (-1)^{\alpha M}}{\pi \left(t - \alpha T_A - \tau_i'\right)/T_A} \tag{10}$$

where

$$a_i = \frac{1}{\prod_{k=0, k\neq i}^{M-1} \sin\left(\pi(\tau_i' - \tau_k')/T_A\right)}, \tag{11}$$

$$\gamma(t) = \prod_{k=0}^{M-1} \sin\left(\pi\left(t - \tau_k'\right)/T_A\right) \tag{12}$$

with $T_A = MT_s$ denoting the period of a single converter and $\tau_k' = kT_s + \tau_k$ is the absolute timing difference from the first converter.

Equation (10) performs perfect reconstruction when no noise is present in the system and sample timings are known precisely. We develop our parameter estimation algorithm for the high signal-to-noise ratio (SNR) regime where $\sigma_w^2 \to 0$, and later introduce the effects of noise on our signal estimation.

In the small mismatch regime, we can approximate (10) by computing the first order Taylor series of the function around the point $\boldsymbol{\tau} = 0$, where vector $\boldsymbol{\tau}$ represents the unknown timing skews

$$\boldsymbol{\tau} = [\tau_1 \ \tau_2 \ \ldots \ \tau_{M-1}]^T. \tag{13}$$

The reconstruction equation reduces at times $t = nT$ to

$$\hat{x}[n] \approx y[n] - \frac{\tau_i}{T_s}(h * y)[n] \quad n(\mathrm{mod}\, M) = i \tag{14}$$

where $*$ represents the convolution operation and

$$h[n] = \begin{cases} 0, & n = 0 \\ \frac{(-1)^n}{n}, & \text{otherwise} \end{cases} \tag{15}$$

is a discrete-time filter implementing bandlimited differentiation. A derivation of (14) is provided in Appendix I. A filterbank implementation of the reconstruction approximation is shown in Fig. 2.

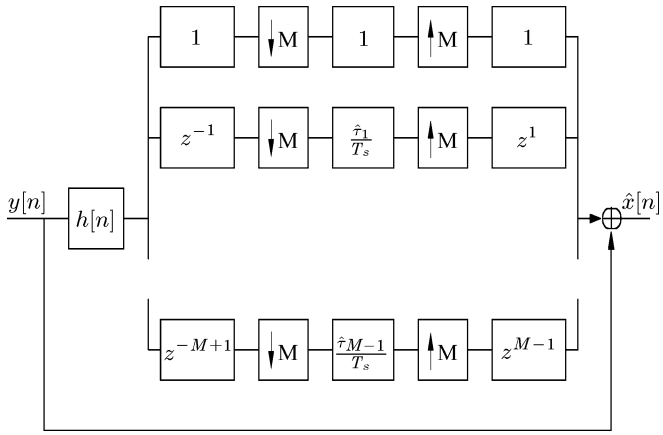

Fig. 2. Signal reconstruction filterbank for a TIADC system from time-skew estimates $\hat{\boldsymbol{\tau}}$ for the small mismatch regime.

Similar to (14), we can also compute the first order expansion of the sinc terms in (5). This yields the received signal equation

$$y[n] \approx x[n] + \frac{\tau_i}{T_s}(h * x)[n] + w[n] \quad n(\mathrm{mod}\ M) = i \quad (16)$$

where $h[n]$ is given in (15). This approximation is useful in subsequent analysis.

C. Matrix Formulation

For convenience, we rewrite our sampling and reconstruction equations in matrix form. Specifically, we write (5) as

$$\boldsymbol{y} = \mathbf{F}\boldsymbol{x} + \boldsymbol{w}. \quad (17)$$

with vectors representing the received TIADC output, the ideal uniform input signal, and the noise signal, i.e.,

$$\boldsymbol{y} = [y[0] \quad y[1] \quad \dots \quad y[N-1]]^T \quad (18)$$
$$\boldsymbol{x} = [x[0] \quad x[1] \quad \dots \quad x[N-1]]^T \quad (19)$$
$$\boldsymbol{w} = [w[0] \quad w[1] \quad \dots \quad w[N-1]]^T \quad (20)$$

and with the matrix

$$\mathbf{F}_{k,l} = \mathrm{sinc}\left((k-l)T_s + \tau_i\right) \quad i = k(\mathrm{mod}\ M) \quad (21)$$

where $0 \le k, l \le N-1$. Note that (17) is a further approximation as we have treated the filter (15) as finite length and neglected edge effects, as is appropriate for larger N. We treat these effects more carefully during simulation.

Next we write (16) as

$$\boldsymbol{y} = \boldsymbol{x} + \sum_{i=1}^{M-1} \frac{\tau_i}{T_s}\mathbf{D}_i\mathbf{H}\boldsymbol{x} + \boldsymbol{w} \quad (22)$$

with $N \times N$ Toeplitz matrix $\mathbf{H}$ representing the filter (15), where $\mathbf{H}_{k,l} = h[k-l]$. The $\mathbf{D}_i$ are $N \times N$ matrices that select the entries from the ith ADC channel,

$$[\mathbf{D}_i]_{k,l} = \begin{cases} 1, & k = l,\ i = k(\mathrm{mod}\ M) \\ 0, & \text{otherwise} \end{cases} \quad (23)$$

where $0 \le k, l \le N-1$. Simplifying (22) further

$$\boldsymbol{y} = (\mathbf{I} + \mathbf{TH})\boldsymbol{x} + \boldsymbol{w} \quad (24)$$

where $\mathbf{T}$ is a diagonal matrix containing the unknown skews

$$\mathbf{T}_{k,l} = \begin{cases} \tau_i/T_s, & k = l,\ k-1(\mathrm{mod}\ M) = i \\ 0, & \text{otherwise} \end{cases} \quad (25)$$

and $\tau_0 = 0$ as stated previously. Eqs. (17) and (24) yield the actual and approximate relationship between $\boldsymbol{x}$ and $\boldsymbol{y}$, respectively.

Similarly, we can rewrite (10) as

$$\boldsymbol{x} = \mathbf{G}\boldsymbol{y} \quad (26)$$

where for $l = \xi(\mathrm{mod}\ M)$

$$\mathbf{G}_{k,l} = \gamma(kT_s)\frac{a_\xi(-1)^{(l-\xi)M}}{\pi\left(kT_s - (l-\xi)T_A - \tau_i'\right)/T_A}. \quad (27)$$

Note that in the absence of noise and neglecting edge effects, (26) performs perfect reconstruction so $\mathbf{G} \approx \mathbf{F}^{-1}$.

The corresponding small mismatch approximation (14) is

$$\boldsymbol{x} = \boldsymbol{y} - \sum_{i=1}^{M-1} \frac{\tau_i}{T_s}\mathbf{D}_i\mathbf{H}\boldsymbol{y} \quad (28)$$
$$= (\mathbf{I} - \mathbf{TH})\boldsymbol{y}. \quad (29)$$

In turn, combining the sampling and reconstruction approximations (24) and (29), we obtain

$$\boldsymbol{x} \approx (\mathbf{I} - \mathbf{THTH})\boldsymbol{x} + (\mathbf{I} - \mathbf{TH})\boldsymbol{w} \quad (30)$$

As expected, in the absence of noise, the reconstruction approximation is accurate up to the second order in $\boldsymbol{\tau}$.

D. Least-Squares Estimation

We estimate the timing skews and input signal using the method of maximum likelihood, modeling the time-skews as nonrandom and unknown parameters. Because the noise $\boldsymbol{w}$ is modeled as white and Gaussian, the maximum-likelihood estimate of the nonrandom unknown parameters $\boldsymbol{x}$ and $\boldsymbol{\tau}$ reduces to the least-squares problem

$$[\hat{\boldsymbol{x}}\ \hat{\boldsymbol{\tau}}] = \underset{\boldsymbol{x}\in\mathcal{S}_B,\boldsymbol{\tau}}{\arg\min} \left\|\boldsymbol{y} - \mathbf{F}(\boldsymbol{\tau})\boldsymbol{x}\right\|^2 \quad (31)$$

where signal estimate

$$\hat{\boldsymbol{x}} = [\hat{x}[0] \quad \hat{x}[1] \quad \dots \quad \hat{x}[N-1]]^T. \quad (32)$$

and where $\mathcal{S}_\mathcal{B}$ captures the bandlimiting constraint, i.e.,

$$\mathcal{S}_B = \{\boldsymbol{x} | \boldsymbol{x} \in \mathcal{R}^N, \mathbf{L}\boldsymbol{x} = \boldsymbol{x}\} \quad (33)$$

with $\mathbf{L}$ implementing a low-pass filter with cutoff ω_c. We explicitly indicate the dependence of $\mathbf{F}$ on $\boldsymbol{\tau}$ in our notation.

We first focus on the estimation of the time-skew parameters then later use these estimates to estimate $\boldsymbol{x}$. It is clear to see that for accurate reconstruction, the estimated signal must be bandlimited, i.e.,

$$\hat{\boldsymbol{x}} = \mathbf{L}\hat{\boldsymbol{x}}. \quad (34)$$

Given the basic least-squares estimator

$$\hat{\boldsymbol{x}} = \mathbf{F}(\boldsymbol{\tau})^{-1}\boldsymbol{y} \quad (35)$$

the bandlimited condition implies that for an accurate of choice of timing skews $\hat{\boldsymbol{\tau}} = \boldsymbol{\tau}$

$$(\mathbf{L} - \mathbf{I})\mathbf{F}(\hat{\boldsymbol{\tau}})^{-1}\boldsymbol{y} = \mathbf{0}. \quad (36)$$

All other choices of $\hat{\boldsymbol{\tau}} \neq \boldsymbol{\tau}$ produce estimates $\hat{\boldsymbol{x}}$ that are not bandlimited (as shown in Appendix II).

In the absence of noise, the timing skews in (36) can be computed from the linear equations attained by using the approximation $\mathbf{F}(\hat{\boldsymbol{\tau}})^{-1} = (\mathbf{I} - \mathbf{TH})$ from (29). In practice, no solution exists due to modeling error in (14) and quantization error; therefore, the optimization is formulated as a least-squares problem that computes the timing skews $\hat{\boldsymbol{\tau}}$ minimizing the out-of-band energy in $\hat{\boldsymbol{x}}$

$$\hat{\boldsymbol{\tau}} = \arg\min_{\boldsymbol{\tau}} \|(\mathbf{L} - \mathbf{I})(\mathbf{I} - \mathbf{TH})\boldsymbol{y}\|^2. \tag{37}$$

Thus, we have reduced the parameter space of the minimization (31) by removing the need to estimate $\boldsymbol{x}$ directly. Rewriting this minimization directly in terms of $\boldsymbol{\tau}$, we get

$$\hat{\boldsymbol{\tau}} = \arg\min_{\boldsymbol{\tau}} \|\boldsymbol{\gamma} - \mathbf{R}\boldsymbol{\tau}\| \tag{38}$$

where

$$\mathbf{R} = [\mathbf{r}_1 \quad \mathbf{r}_2 \quad \dots \quad \mathbf{r}_{M-1}], \quad \mathbf{r}_i = (\mathbf{L} - \mathbf{I})\mathbf{D}_i\mathbf{H}\boldsymbol{y} \tag{39}$$

and

$$\boldsymbol{\gamma} = (\mathbf{L} - \mathbf{I})\boldsymbol{y}. \tag{40}$$

The solution to the over-constrained least-squares estimation problem is given by

$$\hat{\boldsymbol{\tau}} = (\mathbf{R}^T\mathbf{R})^{-1}\mathbf{R}^T\boldsymbol{\gamma}. \tag{41}$$

where the inversion of $\mathbf{R}^T\mathbf{R}$ is possible because for $N \gg M$ and nontrivial $\boldsymbol{y}$, the matrix $\mathbf{R}$ has full column rank. Thus, with $O(M^2N)$ complexity, the optimal solution $\hat{\boldsymbol{\tau}}$ can be computed. Uniform samples of the input signal can then be recovered from the timing skew estimates by methods such as (14).

As discussed previously, the least-squares algorithm is motivated by a desire to calibrate large numbers of converters. It accomplishes this task by requiring a small amount of oversampling in the system and exploiting the extra bandwidth. Because the skews are treated individually (Appendix I), the calibration filters can be fixed and independent of the number of converters, allowing for easy implementation and scaling. The algorithm has many additional benefits. It performs accurate estimation in systems where skews are small in magnitude. The least squares structure allows for a sequential implementation that adapts to changes in the skews (presented subsequently). Also, a large amount of flexibility is available to the system designer in terms of complexity and performance tradeoffs.

A geometric interpretation of the algorithm is that the least-squares method computes the signal in the convex set of signals $\hat{x}[n;\hat{\boldsymbol{\tau}}]$ spanned by $\hat{\boldsymbol{\tau}}$ that is closest to the convex set of signals bandlimited to ω_c. When we introduce back the noise in the system, the estimate deviates from the true value but the estimate error changes in a stable manner with respect to the noise power.

Finally, we discuss two extensions to basic least-squares procedure:

1) Relinearization: For values of τ_i/T_s that are not sufficiently close to zero, the approximation given by (14) may only provide a coarse reconstruction of the original signal because it relies on a Taylor series expansion of (10) around $\boldsymbol{\tau} = \mathbf{0}$. An iterative method for improving the accuracy of the initial least-squares estimate can be derived based on Newton's method. Specifically we perform successive approximations by first computing the least-squares estimate $\hat{\boldsymbol{\tau}}$ and then computing the first order Taylor series approximation of $x[n]$ around the point $\boldsymbol{\tau} = \hat{\boldsymbol{\tau}}$

$$\hat{x}[n] \approx x[n]|_{\boldsymbol{\tau}=\hat{\boldsymbol{\tau}}} + \sum_{i=1}^{M-1} \left.\frac{\partial x[n]}{\partial \tau_i}\right|_{\boldsymbol{\tau}=\hat{\boldsymbol{\tau}}} \tau_i. \tag{42}$$

The explicit computation of (42) is omitted due to its length but is routine. From this updated reconstruction formula, it is possible to formulate a new least-squares problem whose solution is another estimate of $\boldsymbol{\tau}$. With increasingly accurate estimates $\hat{\boldsymbol{\tau}}$, the local approximation of $x[n]$ can improve and allow for better estimation. An alternate approach to achieving increasingly accurate estimates is to incorporate a higher order Taylor series expansion [20].

2) Gains: In the general calibration of time-interleaved analog-to-digital converters, nonuniform gains can also exist among the constituent converters. In this setup, the output of the ith ADC is modeled as

$$y_i[n] = g_i x(nMT_s + iT_s + \tau_i) + w_i[n]. \tag{43}$$

where the g_i are unknown gains. Although the gains vary among the converters, we assume that each gain is within 10% of unity. For high resolution converters, one can conveniently compensate for the system gains without excessive noise enhancement by multiplying each ADC output $y_i[n]$ by $1/g_i$. Without loss of generality, we set $g_0 = 1$.

By folding the gain recovery into the reconstruction equation (10), we can compute the Taylor series approximation around the point $\boldsymbol{\tau} = \mathbf{0}$, $\mathbf{g} = \mathbf{1}$, where

$$\mathbf{g} = [g_1 \quad g_2 \quad \dots \quad g_{M-1}]^T \tag{44}$$

and $\mathbf{0}$, $\mathbf{1}$ are vectors of zeros and ones, respectively. From the first-order approximation, we can setup a similar least-squares problem that includes gains in the vector of unknown parameters

$$\hat{\boldsymbol{\theta}} = \arg\min_{\boldsymbol{\theta}} \|\boldsymbol{\gamma} - \mathbf{R}\boldsymbol{\theta}\| \tag{45}$$

where

$$\boldsymbol{\theta} = \begin{bmatrix} \boldsymbol{\tau} \\ \mathbf{g}' \end{bmatrix} \tag{46}$$

$$\mathbf{R} = [\mathbf{r}_1 \quad \dots \quad \mathbf{r}_{M-1} \quad \mathbf{s}_1 \quad \dots \quad \mathbf{s}_{M-1}] \tag{47}$$

$$\mathbf{r}_i = (\mathbf{L} - \mathbf{I})\mathbf{D}_i\mathbf{H}\boldsymbol{y}, \quad \mathbf{s}_i = -(\mathbf{L} - \mathbf{I})\mathbf{D}_i\boldsymbol{y} \tag{48}$$

$$\boldsymbol{\gamma} = (\mathbf{L} - \mathbf{I})\mathbf{D}_0\boldsymbol{y} \tag{49}$$

and

$$\mathbf{g}' = \left[\frac{1}{g_1} \quad \frac{1}{g_2} \quad \dots \quad \frac{1}{g_{M-1}}\right]^T. \tag{50}$$

The least-squares estimate of the unknown gains and timing skews is

$$\hat{\boldsymbol{\theta}} = (\mathbf{R}^T\mathbf{R})^{-1}\mathbf{R}^T\boldsymbol{\gamma}. \tag{51}$$

Again, in this case further relinearization techniques can allow for an increase in performance.

E. Adaptive Filter Implementation

In the development of the least-squares calibration algorithms, it was convenient to use vectors to represent time-domain signals and matrices to represent filtering operations. This notation allows for greater insight into the methods developed for parameter estimation and signal reconstruction.

In practice, the block implementation of such a system may be cumbersome for efficient implementation as it requires the multiplication of large matrices. As mentioned earlier, FIR filters may be used to replace the matrix operations, such as those discussed in [13], [14], [20], [21]. For example, reconstruction (29) can be simplified through the FIR derivative filter presented in (14). Also, the time skew estimation can be implemented in a sequential manner via an adaptive filter structure, which we now develop.

The block implementation of the timing skew estimate (41) takes $O(M^2N)$ complexity and a large amount of memory. We develop a recursive least-squares (RLS) implementation that distributes the computation over time and adapts to shifts in parameters. To start, we rewrite the matrix $\mathbf{R}$ in terms of its rows $\mathbf{u}$, where each row now represents signal values at a certain time step

$$\mathbf{R} = \begin{bmatrix}\mathbf{u}[0]^T & \mathbf{u}[1]^T & \dots & \mathbf{u}[N-1]^T\end{bmatrix}^T \tag{52}$$

$$\mathbf{u}[n] = \begin{bmatrix}r_1[n] & r_2[n] & \dots & r_{M-1}[n]\end{bmatrix} \tag{53}$$

where $r_i[n]$ is the nth element of $\mathbf{r}_i$. The values can also be computed by the filtering operations

$$r_i[n] = \sum_{m(\mathrm{mod}\ M)=i} p[n-m]s[m] \tag{54}$$

where p implements the high-pass filter $(\mathbf{I}-\mathbf{L})$ and $s[n] = (h*y)[n]$. Also, the vector $\boldsymbol{\gamma}$ in (40) can be written as individual elements $\boldsymbol{\gamma}[n]$, where $\boldsymbol{\gamma}[n] = (p*y)[n]$.

In the recursive setup [24], at time step n, we use $\mathbf{u}[n]$ and $\boldsymbol{\gamma}[n]$ in order to update our filter taps (timing skews). We define a forgetting factor λ such that the weight of the $(n-i)$th sample is λ^{-i}, where $\lambda = 1$ yields the traditional least squares estimate. We also define a regularization constant δ to stabilize the solution. The recursive solution to the least-squares estimation (51) is given by

RLS Initialization

$$\hat{\boldsymbol{\tau}}[0] = \mathbf{0} \tag{55}$$

$$\mathbf{P}[0] = \delta\mathbf{I} \tag{56}$$

RLS Update

$$\boldsymbol{\pi}[n] = \mathbf{P}[n-1]\mathbf{u}[n] \tag{57}$$

$$\mathbf{k}[n] = \frac{\boldsymbol{\pi}[n]}{\lambda + \mathbf{u}^T[n]\boldsymbol{\pi}[n]} \tag{58}$$

$$\xi[n] = \boldsymbol{\gamma}[n] - \hat{\boldsymbol{\tau}}^T[n-1]\mathbf{u}[n] \tag{59}$$

$$\hat{\boldsymbol{\tau}}[n] = \hat{\boldsymbol{\tau}}[n-1] + \mathbf{k}[n]\xi[n] \tag{60}$$

$$\mathbf{P}[n] = \lambda^{-1}\mathbf{P}[n-1] - \lambda^{-1}\mathbf{k}[n]\mathbf{u}^T[n]\mathbf{P}[n-1] \tag{61}$$

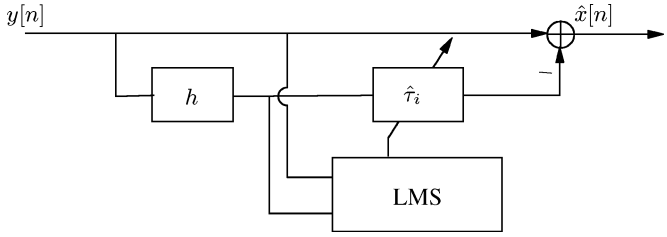

Fig. 3. System implementation of the LMS adaptive filter for timing skew estimation.

where $\mathbf{P}$ represents an estimate of the input $\mathbf{u}$ auto-correlation, which aids in whitening.

The adaptive filter both spreads the computational complexity across time and handles time skews that vary with time. Instead of $O(M^2N)$ complexity every N samples, we now have $O(M^2)$ complexity every sample. Using $\delta = 0.01$ and $\lambda = 1$, we find that the performance of the block algorithm is matched after the steady state is reached.

In practice, the RLS algorithm above is often replaced by the lower complexity least mean-squares (LMS) algorithm. In LMS, no estimation of the covariance matrix $\mathbf{P}$ is made. Instead the $\hat{\boldsymbol{\tau}}$ estimates are updated by the gradient direction that minimizes the $\xi[n]$ error

LMS Update

$$\xi[n] = \boldsymbol{\gamma}[n] - \hat{\boldsymbol{\tau}}^T[n-1]\mathbf{u}[n] \tag{62}$$

$$\hat{\boldsymbol{\tau}}[n] = \hat{\boldsymbol{\tau}}[n-1] + \mu\mathbf{u}[n]\xi[n] \tag{63}$$

where μ denotes the step-size parameter of the update. Fig. 3 shows a system implementation of the reconstruction algorithm.

While the convergence rate of LMS is generally slower than RLS, the LMS algorithm only requires $O(M)$ complexity per sample, making it more attractive for system implementations. In simulations performed with a sufficiently small step-size, the algorithm converged to the same skew estimates as the LS and RLS methods.

III. Signal Reconstruction

We have developed methods for estimating the unknown timing skew parameters. In this section, we present multiple methods for recovering the input $\boldsymbol{x}$ when the timing skews are known (or have been estimated).

In the setup, input $\boldsymbol{x}$ is treated as a nonrandom parameter in

$$\boldsymbol{y} = \mathbf{F}(\boldsymbol{\tau})\boldsymbol{x} + \boldsymbol{w} \tag{64}$$

where we assume $\boldsymbol{\tau}$ is known to the system. We focus on maximum-likelihood estimates of $\boldsymbol{x}$, corresponding to least-square solutions.

A. Naive Least-Squares Estimation

The least-squares (LS) estimate for the input signal is

$$\hat{\boldsymbol{x}}_{\mathrm{LS}} = \arg\min_{\boldsymbol{x}} \|\boldsymbol{y} - \mathbf{F}(\boldsymbol{\tau})\boldsymbol{x}\|^2 \tag{65}$$

where $\boldsymbol{x}$ is bandlimited, a constraint we ignore for the moment. Because the noise $\boldsymbol{w}$ is modeled as white Gaussian, the LS estimate is equivalent to the ML estimate. This formulation is sim-

ilar to the LS setup (31) used to derive the small mismatch estimation algorithm in Section II. In this case, we focus on signal estimation rather than parameter estimation.

The LS solution is equal to

$$\hat{\boldsymbol{x}}_{\mathrm{LS}} = (\mathbf{F}^T\mathbf{F})^{-1}\mathbf{F}^T\boldsymbol{y} \tag{66}$$

$$= \mathbf{F}^{-1}\boldsymbol{y} \tag{67}$$

since $\mathbf{F}$ is invertible when the τ_i are sufficiently small.

This estimation method is equivalent to the reconstruction (10). The estimate performs well in high SNR situations. However, as noise power increases, it is clear to see that this estimate is suboptimal. A more accurate estimate of $\boldsymbol{x}$ can be produced by enforcing the bandlimited constraint on the estimator $\hat{\boldsymbol{x}}$. Because the passband and out-of-band frequencies are orthogonal, this will not affect any signal content in the passband. The final estimate is computed by low-pass filtering the LS estimate. We label this as the filtered least-squares (FLS) estimator

$$\hat{\boldsymbol{x}}_{\mathrm{FLS}} = \mathbf{L}\mathbf{F}^{-1}\boldsymbol{y}. \tag{68}$$

where $\mathbf{L}$ is a matrix implementing a low-pass filter bandlimited to ω_c. This naive estimation technique uses a standard nonuniform reconstruction filter to estimate $\boldsymbol{x}$ from $\boldsymbol{y}$ and then low-pass filters the output to remove any noise in the out-of-band spectrum.

By plugging in for $\boldsymbol{y}$ in the estimator, we find

$$\hat{\boldsymbol{x}}_{\mathrm{FLS}} = \mathbf{L}\mathbf{F}^{-1}(\mathbf{F}\boldsymbol{x} + \boldsymbol{w}) \tag{69}$$

$$= \boldsymbol{x} + \mathbf{L}\mathbf{F}^{-1}\boldsymbol{w}. \tag{70}$$

Thus the error term equals $\mathbf{e}_{\mathrm{FLS}} = \mathbf{L}\mathbf{F}^{-1}\boldsymbol{w}$.

B. Constrained Least-Squares Estimation

We now develop a more accurate estimator by imposing the bandlimited requirement directly into the least-squares estimation. The constrained least-squares (CLS) optimization problem is given by

$$\hat{\boldsymbol{x}}_{\mathrm{CLS}} = \underset{\boldsymbol{x}\in\mathcal{S}_B}{\arg\min} \|\boldsymbol{y} - \mathbf{F}(\boldsymbol{\tau})\boldsymbol{x}\|^2 \tag{71}$$

where $\mathcal{S}_{\mathcal{B}} = \{\boldsymbol{x} | \boldsymbol{x} \in \mathcal{R}^N, \mathbf{L}\boldsymbol{x} = \boldsymbol{x}\}$.

By introducing a secondary variable $\mathbf{z}$, where $\boldsymbol{x} = \mathbf{L}\mathbf{z}$, we can remove the constraint in the LS formulation

$$\hat{\boldsymbol{z}}_{\mathrm{CLS}} = \underset{\mathbf{z}}{\arg\min} \|\boldsymbol{y} - \mathbf{F}\mathbf{L}\mathbf{z}\|^2 \tag{72}$$

$$\hat{\boldsymbol{x}}_{\mathrm{CLS}} = \mathbf{L}\hat{\boldsymbol{z}}_{\mathrm{CLS}}. \tag{73}$$

First, we must compute $\hat{\boldsymbol{z}}_{\mathrm{CLS}}$. Because the matrix $\mathbf{L}$ is singular (high frequency vectors lie in the nullspace), the product matrix $\mathbf{FL}$ is also singular. Thus, it is not possible to take the inverse of this matrix in order to compute the maximum-likelihood estimate $\hat{\boldsymbol{z}}_{\mathrm{CLS}}$. Instead, we use the pseudoinverse

$$\hat{\boldsymbol{z}}_{\mathrm{CLS}} = (\mathbf{FL})^{\dagger}\boldsymbol{y} \tag{74}$$

where $(\cdot)^{\dagger}$ denotes the Moore–Penrose pseudoinverse [25]. The overall solution is given as

$$\hat{\boldsymbol{x}}_{\mathrm{CLS}} = \mathbf{L}(\mathbf{FL})^{\dagger}\boldsymbol{y}. \tag{75}$$

We now analyze this estimator. The low-pass filter matrix can be implemented by a frequency sampling filter matrix, i.e.,

$$\mathbf{L} = \mathbf{D}^{-1}\boldsymbol{\Sigma}_L\mathbf{D} \tag{76}$$

where $\mathbf{D}$ is the $N \times N$ DFT matrix, and $\boldsymbol{\Sigma}_L$ is the frequency response of the filter. Since $\mathbf{L}$ represents a low-pass filter with cutoff frequency ω_c, this is equivalent to having the $(N-k)$ eigenvalues that correspond to the low frequency eigenvectors equal to one and the k eigenvalues that correspond to high frequency eigenvectors equal to zero, where $k = N(\pi - \omega_c)/\pi$. The $N \times N$ eigenvalue matrix is given by

$$\boldsymbol{\Sigma}_L = \begin{bmatrix} \mathbf{I}_{N-k} & \mathbf{0} \\ \mathbf{0} & \mathbf{0} \end{bmatrix}. \tag{77}$$

The nullspace of $\mathbf{L}$ corresponds to linear combinations of high frequency vectors.

The pseudoinverse of $\mathbf{L}$ is equivalent to inverting all the nonzero eigenvalues. Because each of these eigenvalues is equal to one, their inverses are equal to one (and the zero eigenvalues remain zero). Thus, we find that $\mathbf{L}^{\dagger} = \mathbf{L}$. Note that without the frequency sampling approximation (76), the matrix $\mathbf{L}$ may have very small nonzero eigenvalues. When the matrix is inverted, these eigenvalues become very large but can be negated with a power constraint on $\hat{\boldsymbol{x}}$.

To analyze the properties of the product $\mathbf{FL}$, we compute the singular value decomposition

$$\mathbf{FL} = \mathbf{U}\boldsymbol{\Sigma}_{FL}\mathbf{V}^T \tag{78}$$

where $\mathbf{U}$ and $\mathbf{V}$ are $N \times N$ orthonormal matrices. It is easy to see that because $\mathbf{F}$ is full rank, the nullspace $\mathcal{N}(\mathbf{FL}) = \mathcal{N}(\mathbf{L})$ and has rank k. Thus, $\boldsymbol{\Sigma}_{FL}$ can be decomposed as

$$\boldsymbol{\Sigma}_{FL} = \begin{bmatrix} \boldsymbol{\Sigma}_S & \mathbf{0} \\ \mathbf{0} & \mathbf{0} \end{bmatrix} \tag{79}$$

where $\boldsymbol{\Sigma}_S$ is an $(N-k) \times (N-k)$ diagonal matrix.

The bottom k rows of $\mathbf{V}^T$ span the high-frequency nullspace of $\mathbf{L}$, and the top rows span the low-frequency space. Again, since $(\mathbf{FL})^{\dagger}$ inverts only the nonzero eigenvalues, we find that

$$(\mathbf{FL})^{\dagger}\mathbf{FL} = \mathbf{V}\boldsymbol{\Sigma}_L\mathbf{V}^T \tag{80}$$

$$= \mathbf{L} \tag{81}$$

where the second equality holds because the nullspaces of $\mathbf{FL}$ and $\mathbf{L}$ are equal and the low frequency subspace has unity eigenvalues. This simplification does not imply anything about the product $\mathbf{FL}(\mathbf{FL})^{\dagger}$. For similar reasons, it is easy to see that $\mathbf{L}(\mathbf{FL})^{\dagger} = (\mathbf{FL})^{\dagger}$.

From the analysis above, we can better interpret the CLS estimator. First, the received signal is projected into the space of

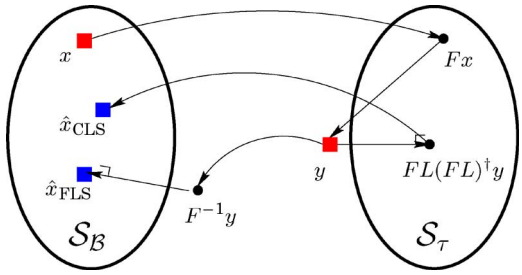

Fig. 4. Graphical representation of the estimator operations. Set $\mathcal{S}_{\mathcal{B}}$ represents the convex set of bandlimited signals. Set $\mathcal{S}_{\tau}$ represents the convex set of signals that can be written as $(\mathbf{F}s)$, where $s \in \mathcal{S}_{\mathcal{B}}$.

$\boldsymbol{\tau}$-spaced periodic nonuniform samples of any possible bandlimited signal, i.e., the space spanned by $\mathbf{FL}$. This produces the intermediate estimate $\mathbf{FL}(\mathbf{FL})^{\dagger}\boldsymbol{y}$. The nonuniform sampling is then inverted by applying $\mathbf{F}^{-1}$. Thus, the noise reduction occurs on the nonuniform samples before the signal reconstruction. Fig. 4 shows a graphical representation of the operations of the estimators.

This approach provides a more efficient method for noise reduction than the equivalent frequency-domain techniques for signal estimation, which are not as easily realizable in hardware. It also provides insight into optimal methods for treating noise when developing practical reconstruction filters.

To compute the CLS estimator error, we substitute for $\boldsymbol{y}$ in (75) and find

$$\hat{\boldsymbol{x}}_{\mathrm{CLS}} = \mathbf{L}(\mathbf{FL})^{\dagger}(\mathbf{F}\boldsymbol{x} + \boldsymbol{w}) \tag{82}$$

$$= \boldsymbol{x} + (\mathbf{FL})^{\dagger}\boldsymbol{w}. \tag{83}$$

The error term equals $\mathbf{e}_{\mathrm{CLS}} = (\mathbf{FL})^{\dagger}\boldsymbol{w}$.

C. Analysis of Estimators

In this section, we analyze the bias, variance, and efficiency of the estimators. From (70) and (83), it is clear that estimators FLS and CLS are unbiased, i.e., $E[\hat{\boldsymbol{x}}] = \boldsymbol{x}$, because the expectation of any linear combination of $w[n]$ is zero.

In order to determine which estimator has lower error variance, we must compare the average error from the covariance matrices

$$\sigma^2_{\mathrm{FLS}} = \frac{1}{N}\sigma^2 \mathrm{tr}\left(\mathbf{L}(\mathbf{F}^T\mathbf{F})^{-1}\mathbf{L}^T\right) \tag{84}$$

$$\sigma^2_{\mathrm{CLS}} = \frac{1}{N}\sigma^2 \mathrm{tr}\left((\mathbf{FL})^{\dagger}(\mathbf{FL})^{\dagger^T}\right). \tag{85}$$

Because comparing the errors is not analytically tractable, we numerically calculate them in Section IV and verify that $\sigma^2_{\mathrm{CLS}} < \sigma^2_{\mathrm{FLS}}$ as expected.

An estimator is efficient if its error variance achieves the Cramer–Rao bound (CRB). In [26], the CRB is redefined for constrained parameter estimation problems. For the problem of

$$\hat{\boldsymbol{x}}_{\mathrm{ML}} = \underset{\boldsymbol{x}, g(\boldsymbol{x})=0}{\arg\max}\, p_{\boldsymbol{y}|\boldsymbol{x}}(\boldsymbol{y}|\boldsymbol{x}) \tag{86}$$

where the $g(\cdot)$ function may contain multiple nonlinear equations, the constrained CRB bound is given by

$$\boldsymbol{\Lambda}_{\hat{\boldsymbol{x}}} \geq \mathbf{J}^{-1} - \mathbf{J}^{-1}\mathbf{G}(\mathbf{G}^T\mathbf{J}^{-1}\mathbf{G})^{-1}\mathbf{G}^T\mathbf{J}^{-1} \tag{87}$$

where

$$\mathbf{J} = -E\left[\nabla_{\boldsymbol{x}} \ln p_{\boldsymbol{y}|\boldsymbol{x}}(\boldsymbol{y}|\boldsymbol{x}) \cdot \nabla^T_{\boldsymbol{x}} \ln p_{\boldsymbol{y}|\boldsymbol{x}}(\boldsymbol{y}|\boldsymbol{x})\right] \tag{88}$$

is the Fisher information matrix and

$$\mathbf{G} = \nabla_{\boldsymbol{x}} g^T(\boldsymbol{x}) \tag{89}$$

is the $N \times N$ gradient matrix of the constraints. In the time interleaved converter setup, the constraints enforce that the estimate is bandlimited, $g(\boldsymbol{x}) = (\mathbf{I} - \mathbf{L})\boldsymbol{x}$. We find

$$\mathbf{J} = \mathbf{F}^T\mathbf{F} \tag{90}$$

$$\mathbf{G} = (\mathbf{I} - \mathbf{L})^T \tag{91}$$

yielding the bound on $\Lambda_{\hat{\boldsymbol{x}}}$ given in (87). Thus, we have the individual variance bound as

$$\mathrm{var}\,[\hat{\boldsymbol{x}}_i(\boldsymbol{y})] \geq [\boldsymbol{\Lambda}_{\hat{\boldsymbol{x}}}]_{i,i}. \tag{92}$$

It is clear that the CLS estimate will achieve the CRB for the constrained ML problem because the constraints are linear. Therefore, by incorporating the bandlimited constraint into the LS estimation, we create an unbiased estimator $\hat{\boldsymbol{x}}_{\mathrm{CLS}}$ that performs better than the naive "reconstruct-and-filter" estimator $\hat{\boldsymbol{x}}_{\mathrm{FLS}}$.

D. Full LS Estimation

The construction of the signal estimate when $\boldsymbol{\tau}$ is known leads us to revisit the timing skew estimation problem. The overall LS estimation (31) of signal and skews can be split into two separate minimizations

$$[\hat{\boldsymbol{x}}\ \hat{\boldsymbol{\tau}}] = \underset{\boldsymbol{x}\in\mathcal{S}_B, \boldsymbol{\tau}}{\arg\min} \|\boldsymbol{y} - \mathbf{F}(\boldsymbol{\tau})\boldsymbol{x}\|^2 \tag{93}$$

$$= \underset{\boldsymbol{\tau}}{\arg\min} \underset{\boldsymbol{x}\in\mathcal{S}_B}{\arg\min} \|\boldsymbol{y} - \mathbf{F}(\boldsymbol{\tau})\boldsymbol{x}\|^2 \tag{94}$$

$$= \underset{\boldsymbol{\tau}}{\arg\min} \left\|\left(\mathbf{I} - \mathbf{FL}(\mathbf{FL})^{\dagger}\right)\boldsymbol{y}\right\|^2. \tag{95}$$

Using the Taylor approximation (29), the estimation of the timing skews becomes

$$\hat{\boldsymbol{\tau}} = \underset{\boldsymbol{\tau}}{\arg\min} \left\|\left(\mathbf{I} - (\mathbf{I} - \mathbf{TH})\mathbf{L}\left((\mathbf{I} - \mathbf{TH})\mathbf{L}\right)^{\dagger}\right)\boldsymbol{y}\right\|^2. \tag{96}$$

Because this minimization is the ML solution, it is guaranteed to have better performance than the method for estimating timing skews in Section II-D. However, the nonlinear characteristics of the pseudoinverse make this estimation method difficult to implement in practice; thus we use it only to provide insight into estimation process.

Fig. 4, which represented the operations of the FLS and CLS estimators, can also help illustrate the timing skew estimation techniques (37) and (96). The ML estimate provided above seeks to find skews $\hat{\boldsymbol{\tau}}$ that minimizes the distance between the

signals y and its projection into $\mathcal{S}_{\hat{\tau}}$, i.e. $\mathbf{F}(\hat{\boldsymbol{\tau}})\mathbf{L}(\mathbf{F}(\hat{\boldsymbol{\tau}})\mathbf{L})^{\dagger}y$, where $\mathbf{F}(\hat{\boldsymbol{\tau}})$ explicitly depends on $\hat{\boldsymbol{\tau}}$. Because this is difficult to compute, we instead find skews $\hat{\boldsymbol{\tau}}$ that minimize the distance between $\mathbf{F}(\hat{\boldsymbol{\tau}})^{-1}y$ and $\hat{x}_{\mathrm{FLS}} = \mathbf{L}\mathbf{F}(\hat{\boldsymbol{\tau}})^{-1}y$.

IV. Results

In this section, we numerically evaluate the performance characteristics of the blind calibration methods. We compare the effective number of bits for the reconstruction without calibration $y[n]$, to the reconstruction with calibration, i.e., $\hat{x}[n]$.

To measure effective bits, we first compute the SNR of the recovered signal $\hat{x}[n]$

$$\mathrm{SNR}_{\hat{x}} = 10\log_{10}\frac{\sum x[n]^2}{\sum (x[n]-\hat{x}[n])^2}. \tag{97}$$

The uncalibrated signal SNR can be calculated in a similar fashion. The effective SNR of a signal is then related to the number of effective bits via $B = (\mathrm{SNR} - 1.76)/6.02$. In the tests below, the converter quantizes the input at 12-bit resolution, which generates the noise $w_i[n]$; the performance is measured through the increase in effective bits between the uncalibrated and calibrated signals. We now discuss the trade-offs in performance between the amount of excess bandwidth, block size, number of converters, and input SNR.

A. Time Skew Calibration

For our simulations, we randomly select the $M-1$ converter timing skews independently using a uniform distribution. Increasing the range of this distribution yields a lower number of effective bits in the uncalibrated signal $y[n]$. Performance is measured for both small and large magnitude skews. The tests are performed using bandlimited Gaussian noise as input, with block sizes of 2^{15} samples and a factor of 33% oversampling. The gains are uniform among all converters. For additional precision, the final estimate $\hat{x}[n]$ is produced using the time-skew estimates in the ideal reconstruction formula (10) rather than the estimated reconstruction formula. Due to the high SNR of the 12-bit ADCs, the improvement of the CLS reconstruction method described in Section III will be postponed until later.

Fig. 5 shows the relationship between the timing skew size and effective number of uncalibrated bits for $M = 2$ converter system. The horizontal axis shows the total amount of skew $(|\tau|/T)$ and the vertical axis represents the resulting number of effective bits in the uncalibrated signal $y[n]$. As expected, for increasing amounts of timing skew, the error in the uncalibrated signal increases, thus decreasing the effective number of bits.

We can also calculate these curves analytically by computing

$$\text{Output Bits} = \frac{1}{6.02}10\log\left(\frac{\sigma_x^2}{\frac{1}{M}\sum\left(\frac{\tau_i}{T_s}\right)^2\sigma_d^2+\sigma_w^2}\right) \tag{98}$$

$$\approx k - \frac{20}{6.02}\log\left(\sum\frac{|\tau_i|}{T_s}\right) \tag{99}$$

where σ_x^2 is the power of the input signal and σ_d^2 is the power of the derivative signal $(\partial/\partial t)x(t)|_{t=nT_s}$.

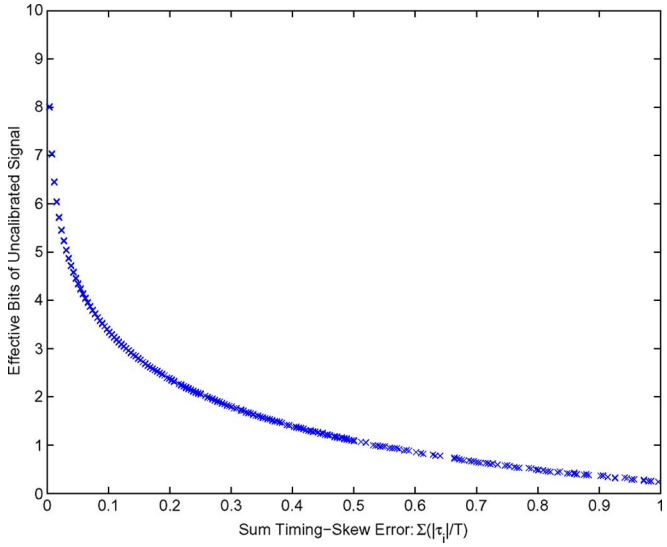

Fig. 5. Effective number of uncalibrated bits versus timing skew value for a 12-bit 2-ADC system. Each "x" on the curve represents a unique test where the timing skew and input signal are chosen at random.

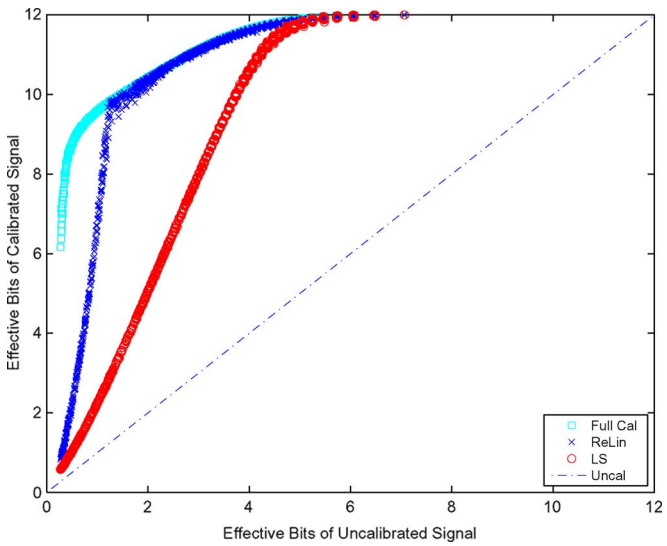

Fig. 6. Effective number of calibrated bits versus uncalibrated bits for a 12-bit 2-ADC system with unknown timing skews. Performance is measured using the least-squares (LS) estimate and the relinearization (ReLin) estimate for a bandlimited Gaussian input oversampled by 33%.

In Figs. 6 and 7, we plot the performance of the small mismatch calibration method by showing the effective bits of the calibrated signal relative to those of the uncalibrated signal for systems with 2 ADCs and 16 ADCs, respectively. For each trial, a random bandlimited Gaussian signal is generated along with a random set of timing skews. The trial signal is calibrated and performance is plotted with a point on each of the curves. Recovery performance is shown for the least-squares "LS" estimate $(\circ)$; and for the 2-ADC system, performance is also shown after multiple relinearization "ReLin" iterations $(\times)$. The number of iterations is approximately equal to $100\tau_1/T_s$.

The full calibration upper bound (squares) shows recovery performance in each trial when the true timing skew values are

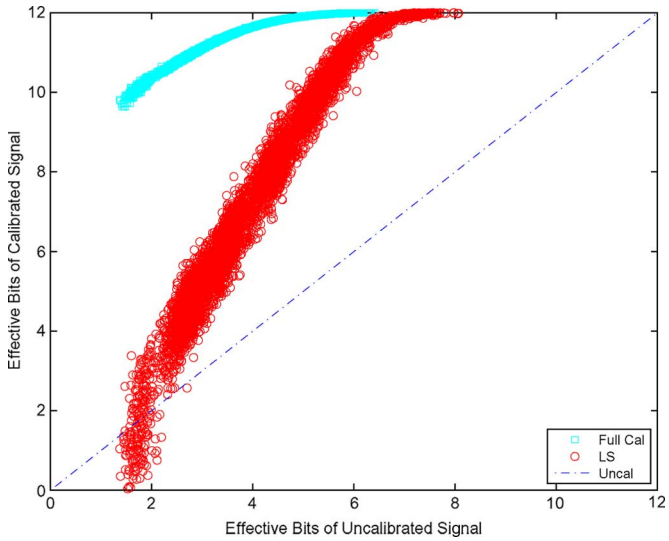

Fig. 7. Effective number of calibrated bits versus uncalibrated bits for a 12-bit 16-ADC system with unknown timing skews. Performance is measured using the least-squares (LS) estimate and the relinearization (ReLin) estimate for a bandlimited Gaussian input oversampled by 33%.

used in the ideal reconstruction formula; note that filter approximations limit the accuracy below 12 effective bits when the skews are large in magnitude (low number of uncalibrated bits). The lower bound (dashed line) plots the performance when no recovery is performed, i.e., effective output bits equals effective input bits.

As the timing skew increases (decreased uncalibrated bits), the recovery algorithm yields a higher number of effective output bits. In the 2-ADC plot, both calibration curves demonstrate a linear behavior until they intersect the upper bound, at which point performance is capped. As the number of calibration iterations increases, the slope of the calibration curve increases. Using the single least-squares calibration, any uncalibrated signal above four effective bits achieves the upper bound. With iterations of the relinearization method, larger timing skews producing signals as low as 1.8 effective bits achieve the same bound. Simulations show the LS performance is limited by how well the reconstruction approximation $(\mathbf{I}-\mathbf{TH})$ performs in comparison to $\mathbf{F}^{-1}$. Thus, the calibration only produces an estimate as good as the reconstruction approximation can yield.

In the 16-ADC system, the performance of the single least-squares calibration matches the full calibration curve for input signals with greater than 5.5 effective bits. Although the relinearization performance is withheld to allow for clarity in the graph, tests show that for uncalibrated signals with more than 4.5 effective bits relinearization achieves the upper bound in performance.

In the time-interleaved setup, sampling generally occurs after the use of an anti-aliasing filter in the analog domain. This filter ensures that high frequencies are not aliased during sampling. Although we model the perfectly sampled signal $x[n]$ to have cutoff frequency ω_c, we cannot guarantee that the signal has nonzero spectral content for $\omega < \omega_c$ or that the spectral content goes to zero for $\omega > \omega_c$, which may lead to degraded performance. If the spectrum is known, this issue can often be resolved by changing the cutoff frequency of the low-pass filter used in skew estimation. However, the spectrum of the input is not always known *a priori*.

We first tested the effects of zero content in a range $\omega_s < \omega < \omega_c$ by using low-pass filters whose cutoff frequencies were (5%, 10%, 20%) larger than the maximum frequency of the signal. In each of the cases, the LS performance remained the same as the base case, while the ReLin performance decreased with larger filter cutoff frequencies. The ReLin degradation was clear for fewer than four uncalibrated bits. For two uncalibrated bits, the (5%, 10%, 20%) cases yielded a ReLin calibration decrease of (0.4, 1.8, 4.0) bits from the base case.

We also tested the effects of nonzero signal in $\omega > \omega_c$ by using inputs that have varying amounts of out-of-band signal content. As a general model for the out-of-band content, we added a white Gaussian signal into this spectrum $(\omega_c < \omega)$ with a power (20, 40, 60)dB lower than the main band $(\omega < \omega_c)$. At -60 dB, the out-of-band energy did not affect calibration performance and at -40 dB, performance only degraded slightly. A -20 dB out-of-band signal yielded a significant drop: for (3,5,7) uncalibrated bits, LS calibration dropped by approximately (2,6,5) bits, respectively. The results of both sets of filtering tests are as expected. Out-of-band signal content can decrease performance by obscuring the aliased content in this band. Also, large filter cutoffs allow for a smaller region for aliasing to be detected, which is only noticeable during relinearization.

Tradeoffs in performance were also measured for varying input block sizes and amounts of oversampling. After a baseline amount of oversampling (15%) and block size (2^{13} samples/ADC), varying these parameters had marginal effects on the LS and ReLin performance, implying that the reconstruction approximation error dominated any out-of-band energy error. However, the convergence speed of the algorithm was highly dependent on the oversampling factor; with more oversampling, fewer relinearization iterations were necessary to achieve the same performance. For 2-ADC systems with 4-bit and 8-bit quantization, the performance curves match the 12-bit curves with upper bound limits performance at 4 bits and 8 bits, respectively. Calibration was also performed using single tone inputs. The trials showed similar performance to the wideband signals; however, tests required that the out-of-band spectrum be specified precisely based on the tone frequency.

The RLS and LMS methods are two possible sequential implementations of the least-squares calibration algorithm. Simulations of the methods were performed using the system parameters of $\delta = 0.001$, $\lambda = 0.95$ for the RLS algorithm and $\mu = 0.05$ for the LMS algorithm. Performance is compared against the block calibration performance with block size $N = 2^{15} = 32768$. For one instance of skews producing block performance of $\sim$7.5 effective bits, tests shows convergence of RLS after 2000 samples and LMS after 15000 samples. By dynamically changing the (λ, μ) parameters over time, we can increase the convergence speed by first using a large stepsize and then using a smaller stepsize. The longer convergence time of the LMS algorithm may be acceptable for high-speed systems due to reduction in complexity.

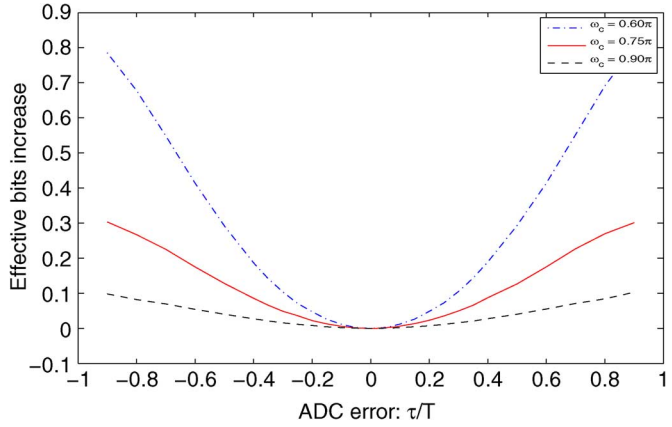

Fig. 8. Effective bits increased by using estimator CLS over FLS in a 2-ADC system for varying amounts of skew. Average performance is plotted for different cutoff frequencies (amounts of oversampling).

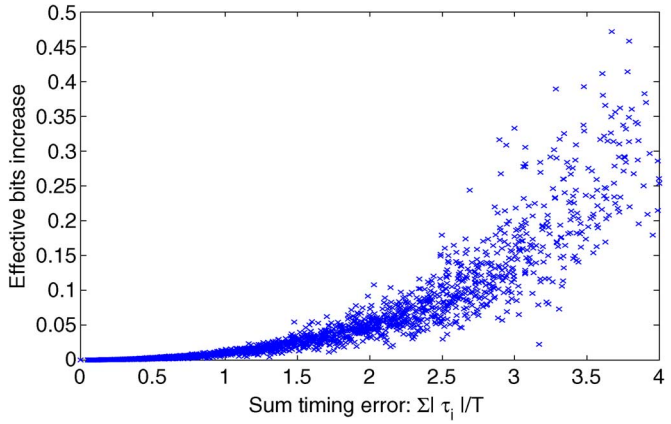

Fig. 9. Effective bits increased by using estimator CLS over FLS in a 16-ADC system with 33% oversampling ($\omega_c = 0.75\pi$). System timing skew is measured by $\sum |\tau_i|/T$. Each x on the plot represents performance in a single test with a randomly chosen set of skews.

To test the tradeoff between complexity and performance, simulations were also conducted with truncated filters. Using the recursive least-squares (RLS) implementation, the filtering processes of $p[n]$ and $h[n]$ were limited to (175,75,30) and (5,10,30) taps respectively. Shortening the high-pass filter p did not significantly change the performance of the LS calibration; however, the ReLin performance decreased with shorter filters. For three uncalibrated bits and the 175 tap $p[n]$, ReLin increased LS performance from 8 to 11 bits, but the 30 tap ReLin remained at 8 bits. The $h[n]$ derivative filter had the opposite effect: LS performance decreased with fewer taps but ReLin performance remained the same. For five uncalibrated bits and the five tap $h[n]$, LS provided six calibrated bits whereas the 30–tap filter yielded 11 calibrated bits. Thus, different system implementations will require a different set of filter lengths based upon the computational power and performance requirements.

Additional tests were performed for signal calibration in time-interleaved systems that contain both unknown timing skews and unknown gains. The $M-1$ gains were chosen independently using a uniform distribution. Although the initial least-squares estimate was often of poor quality, the relinearization technique achieved $\sim$10 bit performance when $M \leq 8$ and the starting number of uncalibrated effective bits is greater than five. This performance is similar to the tests when only timing skews were unknown. For systems with $M = 16$ converters, the gain and skew parameter estimation converged to a local minimum, often not close to the true parameters.

B. Reconstruction Performance

In this section, we present the reconstruction performance of the FLS and CLS estimators developed in Section III by computing the traces of the error covariance matrices of the estimators. As expected, in all cases, the noise power is lower for estimator CLS. The results are given in terms of the increase in effective bits of the CLS estimator over the FLS estimator. We present the performance for varying oversampling ratios and timing skew size in a 12-bit 2-ADC system with block lengths of 512 samples in Fig. 8.

The plot shows that for small amounts of timing skew, the CLS estimate only provides marginal improvements in effective bits. However, the benefits of the estimator are more visible for higher levels of timing skew and oversampling. The effective bit increase is independent of the starting number of effective bits because the signal power remains the same. Thus, the 0.1 bit increase obtained for the 2-ADC system with cutoff $\omega_c = 0.6\pi$ and 30% timing skew holds even for low-resolution converters.

Fig. 9 shows performance in a 16-ADC system for tests where the set of timing skews is chosen at random. The system timing error is measured by the sum of the magnitudes of the timing skews $\sum |\tau_i|/T$. In this case, reconstruction for an average timing skew of $\sim$16% yields a 0.1 bit increase in resolution. Thus, similar performance increases are achieved for the same average timing skew.

V. Conclusion

We have presented a method for the calibration of time-interleaved analog-to-digital converters. The algorithm produces accurate estimates of the unknown system parameters using a least-squares formulation. The estimates are then used to reconstruct samples of the input on a uniform grid. We exploit the linearity of time-skew parameters in high-resolution converters where skews are small relative to the sampling period. The algorithm shows promising performance and its ability to scale easily makes it an attractive solution for large numbers of converters. With the addition of unknown gains and relinearization techniques, the method is robust towards handling a broader class of time-interleaved analog-to-digital converter systems.

For cases of low SNR, the standard method of reconstructing uniform samples from the timing skews can be improved. We presented an alternate approach that incorporates the bandlimited constraint into our reconstruction. The new estimator shows moderate increases in performance for systems with larger timing skews.

The upper bound on the performance of the calibration algorithms needs further investigation. In particular, it is unclear whether accurate convergence of the estimates is guaranteed in the absence of numerical precision errors or algorithmic approximations, especially in the cases of large numbers of converters $M > 32$. An analytic expression for the errors may give insight

into methods for decreasing calibration iterations and increasing estimation accuracy. Also, it may be possible to achieve higher performance by jointly estimating the timing-skews and input signal in the small mismatch least-squares setup.

APPENDIX I
DERIVATION OF THE RECONSTRUCTION EQUATION

We now construct a derivation of the reconstruction approximation (14). We start by computing the Taylor series of the sinc terms in (5). The sinc function at times $t = nT_s + \tau_i$ is equal to

$$\begin{aligned}\operatorname{sinc}(nT_s+\tau_i) &= \operatorname{sinc}(nT_s) + \tau_i \left.\frac{\partial}{\partial t}\operatorname{sinc}(t)\right|_{t=nT_s} && (100)\\ &\quad + O\left(\tau_i^2\right) && (101)\\ &= \begin{cases} \frac{\tau_i}{T_s}\frac{-1^n}{n} + O\left(\tau_i^2\right), & n \neq 0 \\ 1 + O\left(\tau_i^2\right), & n = 0 \end{cases} && (102)\end{aligned}$$

where the function $\operatorname{sinc}(t) = \sin(\pi t/T_s)/(\pi t/T_s)$ is defined with period T_s. Thus the expansion of the sampling equation for $n(\operatorname{mod} M) = i$ becomes

$$\begin{aligned}y[n] &= \sum_m x[m]\operatorname{sinc}\left((n-m)T_s+\tau_i\right) && (103)\\ &= x[n] + \frac{\tau_i}{T_s}(h*x)[n] + O\left(\tau_i^2\right). && (104)\end{aligned}$$

It is easy to see the first order approximation of the inverse reconstruction equation (10) is equal to

$$\begin{aligned}\hat{x}[n] &= y[n] - \frac{\tau_i}{T_s}(h*y)[n] && (105)\\ &= x[n] + O(\boldsymbol{\tau}^2). && (106)\end{aligned}$$

The reconstruction can be realized through a time-varying filter applied to the full TIADC output. In [14], this approximated reconstruction filter is implemented in the $M = 2$ case through a filterbank defined via a Farrow structure. These structures are often used for implementing fractional sample time-delay filters [27], [28].

We now present an alternate derivation that gives the intuition that in our reconstruction formula, we correct each sample by treating all the other samples around it as being sampled uniformly (although this is not actually the case). To show this, we perform an approximation from the interpolation equation $x(t) = \sum x[\alpha]\operatorname{sinc}(t - \alpha T_s)$.

In the absence of noise, for $n(\operatorname{mod} M) = i$:

$$\begin{aligned}x[n] &= \frac{1}{\operatorname{sinc}(\tau_i)} \times \left(y[n] - \sum_{\alpha\neq n} x[\alpha]\operatorname{sinc}\left((n-\alpha)T_s+\tau_i\right)\right) && (107)\\ &\approx \frac{1}{\operatorname{sinc}(\tau_i)} \times \left(y[n] - \sum_{\alpha\neq n} y[\alpha]\operatorname{sinc}\left((n-\alpha)T_s+\tau_i\right)\right) && (108)\\ &\approx y[n] - \frac{\tau_i}{T_s}(h*y)[n] && (109)\end{aligned}$$

where the second approximation is obtained by the first-order Taylor series expansion of the sinc function. Thus, in the correction of a single sample, the derived reconstruction method (14) is equivalent to making the approximation that all the neighbors of the sample are on a uniform grid.

APPENDIX II
UNIQUENESS OF TIMING SKEWS

In the absence of noise, only the true time-skew parameters $\hat{\boldsymbol{\tau}} = \boldsymbol{\tau}$ will yield a reconstructed signal with no out-of-band energy. We start by presenting the reconstruction equation for $M = 2$ ADCs. We show that for $\hat{\boldsymbol{\tau}} \neq \boldsymbol{\tau}$, the output will not be bandlimited. Although the case of $M > 2$ can be proven in a similar manner, we use approximation (14) to simplify the analysis.

We now look at the 2-ADC system and examine the output of the reconstruction filterbank generated by plugging the estimate $\hat{\boldsymbol{\tau}}$ into (10). For simplicity, we assume that the system sampling period $T_s = 1$.

Using $X(e^{j\omega})$ as Fourier transform of the input signal $x[n]$, the ADC outputs are equal to

$$\begin{aligned}Y_0(e^{j\omega}) &= \frac{1}{2}\sum_{k=0}^{1} X\left(e^{j(\omega-2\pi k)/2)}\right) && (110)\\ Y_1(e^{j\omega}) &= \frac{1}{2}\sum_{k=0}^{1} e^{j(\omega-2\pi k)\tau/2} X\left(e^{j(\omega-2\pi k)/2)}\right) && (111)\end{aligned}$$

for $-\pi \leq \omega \leq \pi$.

These signals $Y_0(e^{j\omega})$ and $Y_1(e^{j\omega})$ are now the inputs to our reconstruction filterbank that is constructed from (10). We follow these signals through the filterbank and compute the outputs of each component. We shall use the following notation to represent the two halves (positive/negative frequency) of the Fourier transform

$$\begin{aligned}A^+(e^{j\omega}) &= \begin{cases} A(e^{j\omega}), & \text{for } 0 \leq \omega < \pi \\ 0, & \text{for } -\pi \leq \omega < 0 \end{cases} && (112)\\ A^-(e^{j\omega}) &= \begin{cases} 0, & \text{for } 0 \leq \omega < \pi \\ A(e^{j\omega}), & \text{for } -\pi \leq \omega < 0 \end{cases} && (113)\\ A(e^{j\omega}) &= A^+(e^{j\omega}) + A^-(e^{j\omega}) && (114)\end{aligned}$$

First, the signals are upsampled by a factor of 2, creating signals S_0 and S_1

$$\begin{aligned}S_0(e^{j\omega}) &= \frac{1}{2}\left(X^+\left(e^{j(\omega+\pi)}\right) + X(e^{j\omega}) + X^-\left(e^{j(\omega-\pi)}\right)\right) && (115)\\ S_1(e^{j\omega}) &= \frac{1}{2}\left(X^+\left(e^{j(\omega+\pi)}\right)e^{j(\omega+\pi)\tau} + X(e^{j\omega})e^{j\omega\tau} + X^-\left(e^{j(\omega-\pi)}\right)e^{j(\omega-\pi)\tau}\right) && (116)\end{aligned}$$

for $-\pi \leq \omega \leq \pi$.

Next, the signals $S_0(e^{j\omega})$ and $S_1(e^{j\omega})$ are filtered via $\hat{H}_0(e^{j\omega})$ and $\hat{H}_1(e^{j\omega})$, respectively, producing outputs $R_0(e^{j\omega})$

and $R_1(e^{j\omega})$. The filters, which are computed from the estimate $\hat{\boldsymbol{\tau}}$, are given by

$$\hat{H}_0(e^{j\omega}) = \begin{cases} -\frac{1}{j}a_0\rho, & \text{for } -\pi \le \omega < 0 \\ \frac{1}{j}a_0\rho^{-1}, & \text{for } 0 \le \omega < \pi \end{cases} \tag{117}$$

$$\hat{H}_1(e^{j\omega}) = \begin{cases} \frac{1}{j}a_0\rho^{-1}e^{-j\hat{\tau}\omega}, & \text{for } -\pi \le \omega < 0 \\ -\frac{1}{j}a_0\rho e^{-j\hat{\tau}\omega}, & \text{for } 0 \le \omega < \pi \end{cases} \tag{118}$$

where a_0 is calculated via (11) and $\rho = e^{j\pi\hat{\tau}/2}$.

The reconstructed signal is the sum of $R_0(e^{j\omega})$ and $R_1(e^{j\omega})$:

$$\begin{aligned} &\hat{X}(e^{j\omega}) \\ &= \frac{a_0}{2j}\Big[\left(\rho^{-1} - \rho e^{j(\tau-\hat{\tau})\omega}\right) X^+(e^{j\omega}) && (119)\\ &\quad - \left(\rho - \rho^{-1}e^{j((\tau-\hat{\tau})\omega+\tau\pi)}\right) X^+\left(e^{j(\omega+\pi)}\right) && (120)\\ &\quad - \left(\rho - \rho^{-1}e^{j(\tau-\hat{\tau})\omega}\right) X^-(e^{j\omega}) && (121)\\ &\quad + \left(\rho^{-1} - \rho e^{j((\tau-\hat{\tau})\omega-\tau\pi)}\right) X^-\left(e^{j(\omega-\pi)}\right)\Big]. && (122) \end{aligned}$$

The reconstructed signal will have no "out-of-band" energy if and only if the aliased terms cancel. This is equivalent to ensuring

$$\left(\rho - \rho^{-1}e^{j((\tau-\hat{\tau})\omega+\tau\pi)}\right) X^+\left(e^{j(\omega+\pi)}\right) = 0. \tag{123}$$

Assuming that the aliased signal has content in the out-of-band, we find that for multiple values of ω

$$\begin{aligned} \left(\rho - \rho^{-1}e^{j((\tau-\hat{\tau})\omega+\tau\pi)}\right) &= 0 && (124)\\ -j\pi\hat{\tau}/2 + j\left((\tau-\hat{\tau})\omega + \tau\pi\right) &= j\pi\hat{\tau}/2 && (125)\\ (\tau-\hat{\tau})(\omega+\pi) &= 0 && (126) \end{aligned}$$

which is only true if and only if $\tau = \hat{\tau}$. Thus, if the timing skew estimate is incorrect, the signal is guaranteed to have out-of-band energy.

To generalize to the $M > 2$ converter system, we define the error signal $e[n]$ for an arbitrary estimate $\hat{\boldsymbol{\tau}}$ as follows:

$$\begin{aligned} e[n] &= \hat{x}[n;\boldsymbol{\tau}] - \hat{x}[n;\hat{\boldsymbol{\tau}}] && (127)\\ &= \begin{cases} 0, & n(\mathrm{mod}\ M) = 0 \\ \frac{\hat{\tau}_i - \tau_i}{T_s}(h * y)[n], & n(\mathrm{mod}\ M) = i \end{cases} && (128) \end{aligned}$$

when using approximation formula (14). The reconstruction $\hat{x}[n;\hat{\boldsymbol{\tau}}]$ is bandlimited when $e[n]$ is bandlimited, which is only true if $\hat{\boldsymbol{\tau}} = \boldsymbol{\tau}$ for nontrivial input signals.

REFERENCES

[1] W. C. Black and D. A. Hodges, "Time interleaved converter arrays," *IEEE J. Solid-State Circuits*, vol. 15, pp. 1022–1029, Dec. 1980.

[2] A. Petraglia and S. K. Mitra, "Analysis of mismatch effects among A/D converters in a time-interleaved waveform digitizer," *IEEE Trans. Instrum. Meas.*, vol. 40, no. 5, pp. 831–835, Oct. 1991.

[3] C. Vogel, "The impact of combined channel mismatch effects in time-interleaved ADCs," *IEEE Trans. Instrum. Meas.*, vol. 54, no. 2, pp. 415–427, Feb. 2005.

[4] K. Dyer, D. Fu, S. Lewis, and P. Hurst, "An analog background calibration technique for time-interleaved analog-to-digital converters analog background calibration technique for time-interleaved analog-to-digital converters," *IEEE J. Solid-State Circuits*, vol. 33, no. 12, pp. 1912–1919, Dec. 1998.

[5] S. Jamal, D. Fu, M. Singh, P. Hurst, and S. Lewis, "Calibration of sample-time error in a two-channel time-interleaved analog-to-digital converter," *IEEE Trans. Circuits Syst.*, vol. 51, no. , pp. 130–139, Jan. 2004.

[6] V. Divi and G. Wornell, "Signal recovery in time-interleaved analog-to-digital converters," in *Proc. IEEE ICASSP*, 2004, pp. 593–596.

[7] Y.-C. Jenq, "Digital spectra of nonuniformly sampled signals: A robust sampling time offset estimation algorithm for ultra high-speed waveform digitizers using interleaving," *IEEE Trans. Instrum. Meas.*, vol. 39, no. 1, pp. 71–75, Feb. 1990.

[8] H. Jin and E. K. F. Lee, "A digital-background calibration technique for minimizing timing-error effects in time-interleaved ADCs," *IEEE Trans. Circuits Syst. II*, vol. 47, no. 4, pp. 603–613, Jul. 2000.

[9] V. Divi and G. Wornell, "Scalable blind calibration of timing skew in high-resolution time-interleaved ADCs," in *Proc. IEEE ISCAS*, May 2006, pp. 3390–3393.

[10] V. Divi, "Estimation and calibration algorithms for distributed sampling systems," Ph.D. dissertation, Mass. Inst. of Technology, Cambridge, MA, 2008.

[11] P. Marziliano and M. Vetterli, "Reconstruction of irregularly sampled discrete-time bandlimited signal with unknown sampling locations," *IEEE Trans. Signal Process.*, vol. 48, no. 12, pp. 3462–3471, Dec. 2000.

[12] J. Elbornsson, F. Gustafsson, and J.-E. Eklund, "Blind adaptive equalization of mismatch errors in time-interleaved A/D converter system," *IEEE Trans. Circuits Syst.*, vol. 51, no. 1, pp. 151–158, Jan. 2004.

[13] M. Seo, M. J. W. Rodwell, and U. Madhow, "Blind correction of gain and timing mismatches for a two-channel time-interleaved analog-to-digital converter," in *Proc. 39th Asilomar Conf. Signals, Syst., Comput.*, Oct. 2005, pp. 1121–1125.

[14] S. Huang and B. C. Levy, "Adaptive blind calibration of timing offset and gain mismatch for two-channel time-interleaved ADCs," *IEEE Trans. Circuits Syst. I*, vol. 53, no. 6, pp. 1278–1288, Jun. 2006.

[15] S. Huang and B. C. Levy, "Blind calibration of timing offsets for four-channel time-interleaved ADCs," *IEEE Trans. Circuits Syst. I*, vol. 54, no. 4, pp. 863–876, Apr. 2007.

[16] C. Vogel, "A frequency domain method for blind identification of timing mismatches in time-interleaved ADCs," in *Proc. Norchip Conf.*, Nov. 2006, pp. 45–48.

[17] T. Strohmer and J. Xu, "Fast algorithms for blind calibration in time-interleaved analog-to-digital converters," in *Proc. IEEE ICASSP*, Apr. 2007, pp. 1225–1228.

[18] Y. C. Eldar and A. V. Oppenheim, "Filterbank reconstruction of bandlimited signals from nonuniform and generalized samples," *IEEE Trans. Signal Process.*, vol. 48, no. 10, pp. 2864–2875, Oct. 2000.

[19] H. Johansson and P. Löwenborg, "Reconstruction of nonuniformly sampled bandlimited signals by means of digital fractional delay filters," *IEEE Trans. Signal Proc.*, vol. 50, no. 11, pp. 2757–2767, Nov. 2002.

[20] H. Johansson, P. Löwenborg, and K. Vengattaramane, "Least-squares and minimax design of polynomial impulse response fir filters for reconstruction of two-periodic nonuniformly sampled signals," *IEEE Trans. Circuits Syst. I*, vol. 54, no. 4, pp. 877–888, Apr. 2007.

[21] T. Strohmer and J. Tanner, "Fast reconstruction algorithms for periodic nonuniform sampling with applications to time-interleaved ADCs," in *Proc. IEEE ICASSP*, Apr. 2007, pp. 881–884.

[22] V. Divi and G. Wornell, "Bandlimited signal reconstruction from noisy periodic nonuniform samples in time-interleaved adcs," in *Proc. IEEE ICASSP*, 2008, pp. 3721–3724.

[23] J. Yen, "On nonuniform sampling of bandwidth-limited signals," *IRE Trans. Circuit Theory*, vol. 3, pp. 251–257, Dec. 1956.

[24] S. Haykin, *Adaptive Filter Theory*. Upper Saddle River, NJ: Prentice-Hall, 2002.

[25] G. H. Golub and C. F. Van Loan, *Matrix Computations*. Baltimore, MD: Johns Hopkins Univ. Press, 1996.

[26] J. D. Gorman and A. O. Hero, "Lower bounds for parametric estimation with constraints," *IEEE Trans. Info Theory*, vol. 36, no. 11, pp. 1285–1301, Nov. 1990.

[27] T. I. Laakso, V. Välimäki, M. Karjalainen, and U. K. Laine, "Splitting the unit delay—Tools for fractional delay filter design," *IEEE Signal Process. Mag.*, vol. 13, no. 1, pp. 30–60, Jan. 1996.

[28] F. J. Harris, *Multirate Signal Processing for Communication Systems*. Upper Saddle River, NJ: Prentice-Hall, 2004.

Vijay Divi (S'02–M'08) received the B.S., M.E., and Ph.D. degrees from the Massachusetts Institute of Technology (MIT), Cambridge, in 2002, 2004, and 2008, respectively, all in electrical engineering and computer science.

His research is in the area of distributed sampling algorithms and applications to high-speed A/D conversion and broader interests include topics in signal processing, estimation, optimization, communication systems, and circuit design. Beyond MIT, he has held summer positions at Lincoln Laboratories, Samsung Electronics, Mitsubishi Electric Research Laboratory (MERL), and Akamai Technologies.

Dr. Divi is a recipient of the National Defense Science and Engineering (NDSEG) Fellowship and was awarded the Morris Joseph Levin EECS Masterworks award from MIT.

Gregory W. Wornell (S'83–M'91–SM'00–F'04) received the B.A.Sc. degree from the University of British Columbia, Vancouver, BC, Canada, in 1985 and the S.M. and Ph.D. degrees from the Massachusetts Institute of Technology (MIT), Cambridge, in 1987 and 1991, respectively, all in electrical engineering and computer science.

Since 1991, he has been on the faculty at MIT, where he is a Professor of electrical engineering and computer science, and Co-Director of the Center for Wireless Networking. He has held visiting appointments at the former AT&T Bell Laboratories, Murray Hill, NJ, the University of California, Berkeley, and Hewlett-Packard Laboratories, Palo Alto, CA. His research interests and publications span the areas of signal processing, digital communication, and information theory, and include algorithms and architectures for wireless and sensor networks, broadband systems, and multimedia environments.

Dr. Wornell has been involved in the Information Theory and Signal Processing Societies of the IEEE in a variety of capacities, and maintains a number of close industrial relationships and activities. He has won a number of awards for both his research and teaching.